Eur. Phys. J. E **21**, 319–330 (2006)
DOI 10.1140/epje/i2006-10070-8

THE EUROPEAN PHYSICAL JOURNAL E

Tuneable micro- and nano-periodic structures in a free-standing flexible urethane/urea elastomer film

M.H. Godinho[1,a], A.C. Trindade[1,b], J.L. Figueirinhas[2,3,c], L.V. Melo[3,d], P. Brogueira[3,4,e], A.M. Deus[4,5,f], and P.I.C. Teixeira[6,g]

[1] Departamento de Ciência dos Materiais and CENIMAT, Faculdade de Ciências e Tecnologia, Universidade Nova de Lisboa, P-2829-516 Caparica, Portugal
[2] Centro de Física da Matéria Condensada, Universidade de Lisboa, Avenida Professor Gama Pinto 2, P-1649-003 Lisbon, Portugal
[3] Departamento de Física, Instituto Superior Técnico, Avenida Rovisco Pais, P-1049-001 Lisbon, Portugal
[4] ICEMS, Instituto Superior Técnico, Avenida Rovisco Pais, P-1049-001 Lisbon, Portugal
[5] Departamento de Engenharia de Materiais, Instituto Superior Técnico, Avenida Rovisco Pais, P-1049-001 Lisbon, Portugal
[6] Faculdade de Engenharia, Universidade Católica Portuguesa, Estrada de Talaíde, P-2635-631 Rio de Mouro, Portugal

Received 16 May 2006 and Received in final form 30 October 2006
Published online: 12 February 2007 –

Abstract. We have studied the control and manipulation of tuneable equilibrium structures in a free-standing urethane/urea elastomer film by means of atomic force microscopy, small-angle light scattering and polarising optical microscopy. The urethane/urea elastomer was prepared by reacting a poly(propyleneoxide)-based triisocyanate-terminated prepolymer (PU) with poly(butadienediol) (PBDO), with a weight ratio of 60% PU/40% PBDO. An elastomer film was shear-cast onto a glass plate and allowed to cure, first in an oven, then in air. Latent micro- and nano-periodic patterns are induced by ultra-violet (UV) irradiation of the film and can be "developed" by applying a plane uniaxial stress or by immersing the elastomer in an appropriate solvent and then drying it. For this elastomer we describe six pattern states, how they are related and how they can be manipulated. The morphological features of the UV-exposed film surface can be tuned, reproducibly and reversibly, by switching the direction of the applied mechanical field. Elastomers extracted in toluene exhibit different surface patterns depending upon the state in which they were developed. Stress-strain data collected for the films before and after UV irradiation reveal anisotropy induced by the shear-casting conditions and enhanced by the mechanical field. We have interpreted our results by assuming the film to consist of a thin, stiff surface layer ("skin") lying atop a thicker, softer substrate ("bulk"). The skin's higher stiffness is hypothesised to be due to the more extensive cross-linking of chains located near the surface by the UV radiation. Patterns would thus arise as a competition between the effects of bending the skin and stretching/compressing the bulk, as in the work of Cerda and Mahadevan (Phys. Rev. Lett. **90**, 074302 (2003)). We present some preliminary results of a simulation of this model using the Finite Element package ABAQUS.

PACS. 61.41.+e Polymers, elastomers, and plastics – 62.25.+g Mechanical properties of nanoscale materials – 82.20.Wt Computational modeling; simulation

1 Introduction

Refined, next-generation micromechanical systems require adaptive surfaces constructed with smart properties that can not only sense or respond to environmental stimuli, but also be tough and possess tailored, on-demand topographic properties [1–4]. Techniques for the

[a] e-mail: mhg@fct.unl.pt
[b] *Present address*: Departamento de Química, Instituto Superior Técnico, Avenida Rovisco Pais, P-1049-001 Lisbon, Portugal.
[c] e-mail: figuei@cii.fc.ul.pt
[d] e-mail: lhvm@fisica.ist.utl.pt
[e] e-mail: pedro@fisica.ist.utl.pt
[f] e-mail: amd@ist.utl.pt
[g] *Present address*: Instituto Superior de Engenharia de Lisboa, Rua Conselheiro Emídio Navarro 1, P-1950-062 Lisbon, Portugal; and Centro de Física Teórica e Computacional, Universidade de Lisboa, Avenida Professor Gama Pinto 2, P-1649-003 Lisbon, Portugal; e-mail: piteixeira@cii.fc.ul.pt

micropatterning of soft materials are therefore of great importance for the design of new nanoscale electronic, optical and mechanical devices, ranging from displays [5, 6] and actuators [7] to microfluidics [8] to biomedical materials [9]. Such tecniques should be simple and low-cost, and allow a very precise (and ideally reversible) tuning of system properties. Earlier attempts have included the deposition of metal films on elastomeric polymer substrates [5,7,10–13], swelling of a supported polymer layer [14], heating of a polymer bilayer [15], and layer-by-layer assembly of gold nanoparticle sandwiches [16, 17]. These, however, perforce combine different types of material in sophisticated multi-step processing routines. Ideally one would like to use a single compound —a polymer if possible, in view of its mechanical compliance— and standard laboratory procedures.

Urethane-urea elastomers are a broad and motivating class of polyurethanes that owe their unique elastic properties to the microphase separation of hard (isocyanate) and soft (polyol) segments into domain structures during material preparation and processing [18]. The urethane/urea hard groups usually contain polar functionalities that can form very strong chemical or physical bonds [19]. The tensile properties of polyurethanes are of great importance to their applications, as they can be stretched to many times their initial length and pull back to roughly their original shape and dimensions, and several studies have been carried out on the genesis of structures during their deformation [20]. Urethane/urea polymers are typically linear block copolymers containing urethane/urea groups and chain extenders. Depending on the nature and the proportions of these components, different physical properties can be obtained [21,22]. Block copolymers have been extensively investigated and have proven to be eminently suitable as multipurpose lively materials in nanoscience and nanotechnology [22–25]. They are known for self-assembling at the nanometer length scale with the formation of a variety of highly ordered phases [26], not only in bulk but also upon dilution by a solvent that interacts selectively with one of the constituent blocks [27–29].

The synthesis and preparation have been reported of urethane/urea elastomers with two soft segments, polypropylene oxide and polybutadiene, to make pervaporation membranes with improved permeation performance. ATR-FTIR was used to elucidate the phase behaviour of the urethane/urea groups for these materials and segregation effects/mixing of hard and soft segments were found for membranes with different polybutadiene content [30]. In an earlier paper, we showed that thick (60–100 μm) urethane/urea segmented elastomer films can exhibit, under appropriate conditions, an instability-driven mechanico-optical effect when exposed to daylight for several months, or to UV in a controlled environment for several days [31]. This effect is the appearance of two optical states, corresponding to two distinct periodic surface textures, in the elastomer, upon application of an extensional stress. In the stretched state, the periodic modulation ("stripes") has wave vector in the plane of the sample, perpendicular to the direction of deformation, and a small amplitude: the film looks transparent. If the imposed stress is then removed, the elastomer recovers its original dimensions, the stripes vanish and a new periodic modulation develops with wave vector parallel to the direction along which the film was previously deformed, and an amplitude larger than the stripes ("bands"): it scatters light more efficiently and the film looks translucent [32]. In both cases the wavelength of the modulations is of the order of a few μm, and their amplitudes of the order of tens to hundreds of nm, hence much smaller than the film thickness. Such textures are highly reproducible and remarkably defect-free. The translucent/transparent switching driven by the mechanical field resembles the polydomain/monodomain transition of liquid-crystal elastomers [33] (although our films are not liquid crystalline, as evidenced by their very small birefringence). Moreover, the surface topography of the translucent state after stress removal can be micro-tuned by applying/removing an external uniaxial mechanical field along different directions [34], or by varying the relative proportions of polypropylene and polybutadiene segments present in the elastomer and developed with the solvent [35].

In this paper we expand on our earlier work [31,32] by using atomic force microscopy (AFM), small-angle light scattering (SALS) and polarising optical microscopy (POM) to perform a fully quantitative characterisation of the surface textures of a thin free-standing film, prepared by shear-casting a urethane/urea elastomer made by reacting a poly(propylene oxide)-based triisocyanate terminated prepolymer (PU) with poly(butadienediol) (PBDO) in a weight ratio of 60% PU/40% PBDO. We study how the morphological features observed in the elastomer

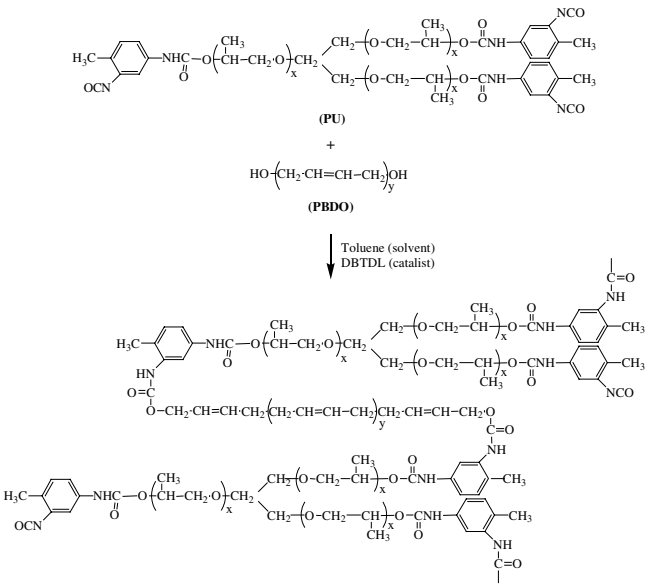

Fig. 1. First chemical synthesis step to form urethane linkages from reaction of the end groups of the tri-functional polypropylene oxide-based isocyanate prepolymer (PU), $x = 20$, with the end groups of polybutadiene diol (PBDO), $y = 50$, catalysed by dibutyl tin dilauryate (DBTDL).

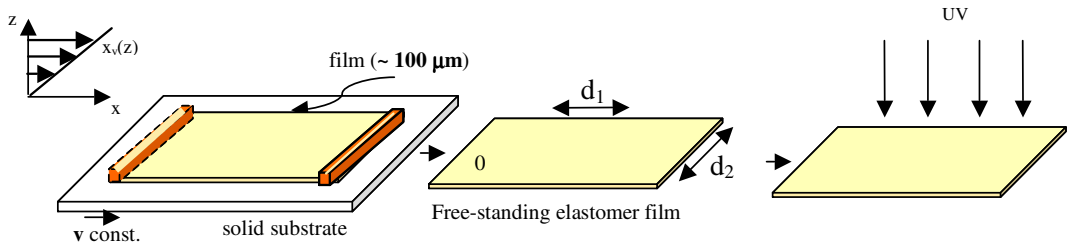

Fig. 2. Schematics of the preparation procedure of poly(propylene oxide)/polybutadiene bi-soft segment urethane/urea thin-solid-film ($\sim 100\,\mu$m) samples. From left to right: the initial solid film is prepared, after 30 min of chemical reaction (see Fig. 1), from a mixture with a solid content of 40 wt% in toluene. The mixture is cast onto a treated glass (solution of 20 wt% of silane in ethanol) and sheared by moving a casting knife at a controlled shear rate ($v = 5$ mm/s), the direction of shear is $\mathbf{d}_1$. The free-standing solid elastomer film is then removed from the treated glass substrate after curing (72 h) in atmospheric moisture (*sample I0*). $\mathbf{d}_2$ is the direction perpendicular to shear ($\mathbf{d}_1$). *Sample II0* is obtained by UV-irradiating *sample I0*.

depend on i) the mechanical treatment of the initial sample and on ii) whether sol/gel extraction was performed or not, which are two standard laboratory procedures. The different states induced in the elastomer by the external mechanical field and by solvent extraction are described and related; it is discussed how they can be manipulated. The effect of the shear-casting conditions on the anisotropic mechanical behaviour of the elastomer is also investigated. Finally, we propose a theoretical model to account for the periodic surface modulations found and present some preliminary results.

2 Experimental

The elastomer was synthesized via two chemical steps between the prepolymers shown in Figure 1, PU and PBDO, according to the procedure described in [31,36].

The PBDO is a mixture of *cis* and *trans* isomers, with glass transition temperatures $-108\,^\circ$C and $-78\,^\circ$C, respectively, and a number-average molecular weight of 2800 g/mol; it was supplied by Aldrich. The PU has a molecular weight of approximately 3500 g/mol, its glass transition temperature is approximately $-75\,^\circ$C in bulk, and $-25\,^\circ$C in a cross-linked film; it was purchased from the Portuguese petrochemical industry (CPB). These prepolymers were recently investigated with regard to their ability to be the chemical precursors of solid films with different nano- to micro-modulated surfaces by tuning their PU/PBDO relative content [30]. In this work we use an excess of PU prepolymer (60% PU/40% PBDO rather than 40% PU/60% PBDO as before [31,32]) in order to obtain a network with two kinds of covalent bonds, with urethane and urea groups: the resulting elastomer is easier to handle, and has two glass transitions at approximately $-35\,^\circ$C and $-65\,^\circ$C [36].

The PU and PBDO prepolymers were dissolved in toluene (solid content 40 wt%) and one drop of dibutyl tin dilauryate (DBTDL) catalyst was added. The reaction of the cyanate end groups of PU with the hydroxyl end groups of PBDO was allowed to proceed for 30 minutes, under a nitrogen atmosphere; a weakly cross-linked urethane network was obtained. The elastomer was then cast and sheared simultaneously onto a glass plate at room temperature, by moving a casting knife at a controlled shear rate ($v = 5$ mm/s) along a direction henceforth denoted $\mathbf{d}_1$, as shown in Figure 2; we also define $\mathbf{d}_2$ as the direction at $90\,^\circ$ to $\mathbf{d}_1$ in the plane of the film.

The resulting elastomer film was then cured in an oven at 70–80 °C for 3.5 h, and subsequently allowed to continue curing for at least 72 h in air. The cross-linking density was thus modified by reaction of the remaining cyanate groups with atmospheric moisture to give urea bonds between the PU units. This was further promoted by the casting-shearing technique. The film was then exposed to UV radiation ($\lambda = 254$ nm) for 4 days. After solvent evaporation and cross-linking the film was carefully removed from the glass-treated substrate. Its final thickness was measured using a Mitutoyo digital micrometer. For all films this was about 100 μm.

Films were cut into 5 cm × 2 cm samples and measurements of their mechanical (tensile) properties were carried out on a Rheometric Scientific (Minimat Firmware version 3.1) testing machine at room temperature. A mechanical property of a given sample was taken to be the average of the results of six successful measurements (see [31] for details). We determined the elastic moduli of the dry urethane/urea films in the two mutually perpendicular directions $\mathbf{d}_1$ and $\mathbf{d}_2$ defined above.

AFM was used to characterise quantitatively the topographical features of the films, before and after application of the mechanical field, and before and after extraction with toluene. A Dimension 3100 SPM with a Nanoscope IIIa controller from Digital Instruments (DI) was employed. Measurements were performed in tapping mode TM under ambient conditions, using a commercial tapping-mode etched silicon probe from DI and a $90 \times 90\,\mu\text{m}^2$ scanner. Besides allowing the capture of 3D images, AFM can also measure a number of parameters that characterise surface topography: if $h(\vec{r})$ is the surface height at point $\vec{r} = (x, y)$, one defines the surface *mean roughness* R_a as

$$R_a = \frac{1}{L_x L_y} \int_0^{L_x} \int_0^{L_y} |h(x,y)| \mathrm{d}x \mathrm{d}y,$$

Table 1. Elastic modulus determined by means of stress-strain measurements at room temperature ($\sim 22\,^{\circ}$C) (nominal stress *vs.* strain) for some of our urethane/urea elastomer (60% PU/40% PBDO). *Sample I0* is an elastomer film before UV irradiation, *sample II0* originates from *sample I0* after UV irradiation, *sample IIA* originates from *sample II0* after extension along $\mathbf{d}_1$ and $\mathbf{d}_2$, *sample IIB* originates from *sample IIA* after extension along $\mathbf{d}_1$. *Sample III-20* originates from *sample II0* after extraction in toluene, *samples III-2A* and *III-2B* originate from, respectively, *samples IIA* and *IIB* after extraction in toluene (see also Figs. 2 and 10).

Urethane/Urea elastomer Sample	UV irradiation	(A) Stresses applied along $\mathbf{d}_1$ and $\mathbf{d}_2$ consecutively and removed	(B) Stress applied along $\mathbf{d}_1$ after cycle A	Extraction in toluene	Elastic modulus along $\mathbf{d}_1$ (MPa)	Elastic modulus along $\mathbf{d}_2$ (MPa)
Sample I0	No	No	No	No	4.22 ± 0.01	2.84 ± 0.01
Sample II0	Yes	No	No	No	4.39 ± 0.02	3.29 ± 0.05
Sample III-20	Yes	No	No	Yes	3.73 ± 0.02	3.76 ± 0.02
Sample III-2A	Yes	Yes	No	Yes	3.93 ± 0.05	3.70 ± 0.01
Sample III-2B	Yes	Yes	Yes	Yes	3.57 ± 0.03	2.47 ± 0.02

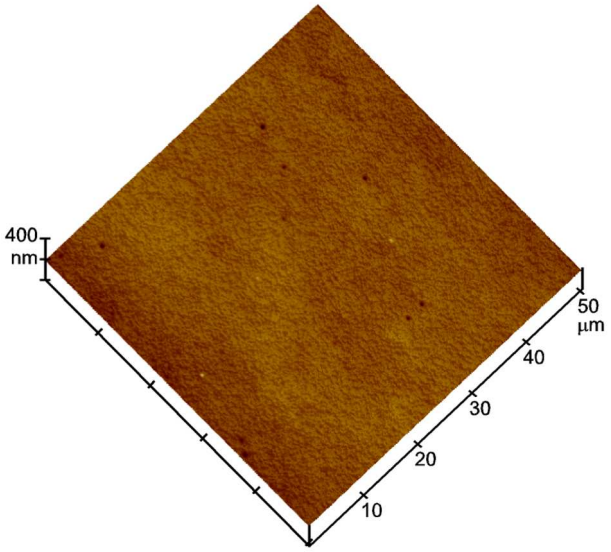

Fig. 3. 3D topography image ($50 \times 50\,\mu\text{m}^2$ scan) of the free surface of *sample II0*. This sample has been UV-irradiated but not subjected to any mechanical stress. Here and in all topography images that follow, the scale on the right is in the plane of the sample, and that on the left is the vertical scale coming out of the plane of the sample. The surface is nanometrically flat, as can be concluded from its roughness parameters listed in Table 2.

and the *root-mean-square roughness* R_q, as

$$R_q = \sqrt{\frac{1}{L_x L_y} \int_0^{L_x} \int_0^{L_y} h^2(x,y) \mathrm{d}x \mathrm{d}y}\,,$$

where L_x, L_y are the scanning window dimensions along x and y, respectively.

Optical micrographs (obtained by POM) were taken with an Olympus polarising microscope equipped with a photographic camera.

Table 2. Roughness parameters as determined by AFM for some of the urethane/urea elastomer films in Figure 10 below (see also Fig. 2).

Urethane/Urea elastomer Sample	Mean roughness R_a (nm)	Root-mean-square roughness R_q (nm)
Sample II0	0.57	0.75
Sample III-20	217	270
Sample III-2A	170	205
Sample IIB	61	73
Sample III-2B	294	392

The small-angle light scattering (SALS) data were obtained on an optical bench equipped with a green ($\lambda = 543.5$ nm) helium-neon laser. SALS patterns were recorded with a CCD video camera. Extraction in toluene was performed using a Soxhlet apparatus for up to 72 hours at $80\,^{\circ}$C, to remove any unreacted products.

Before moving on to discussing our results it is crucial to introduce a convenient notation for describing the various treatments that films have been subjected to.

- *Type-I* films are films as cast, *i.e.*, without any further treatment.
- *Type-II* films are UV-irradiated films.
- *Type-III* films have been extracted in toluene for 72 h and then dried. They divide into two subtypes:
  - *Type-III-1* films are films extracted in toluene but not UV-irradiated (*i.e.*, they were obtained by extracting type-I films in toluene).
  - *Type-III-2* films are films extracted in toluene after UV irradiation (*i.e.*, they were obtained by extracting type-II films in toluene).

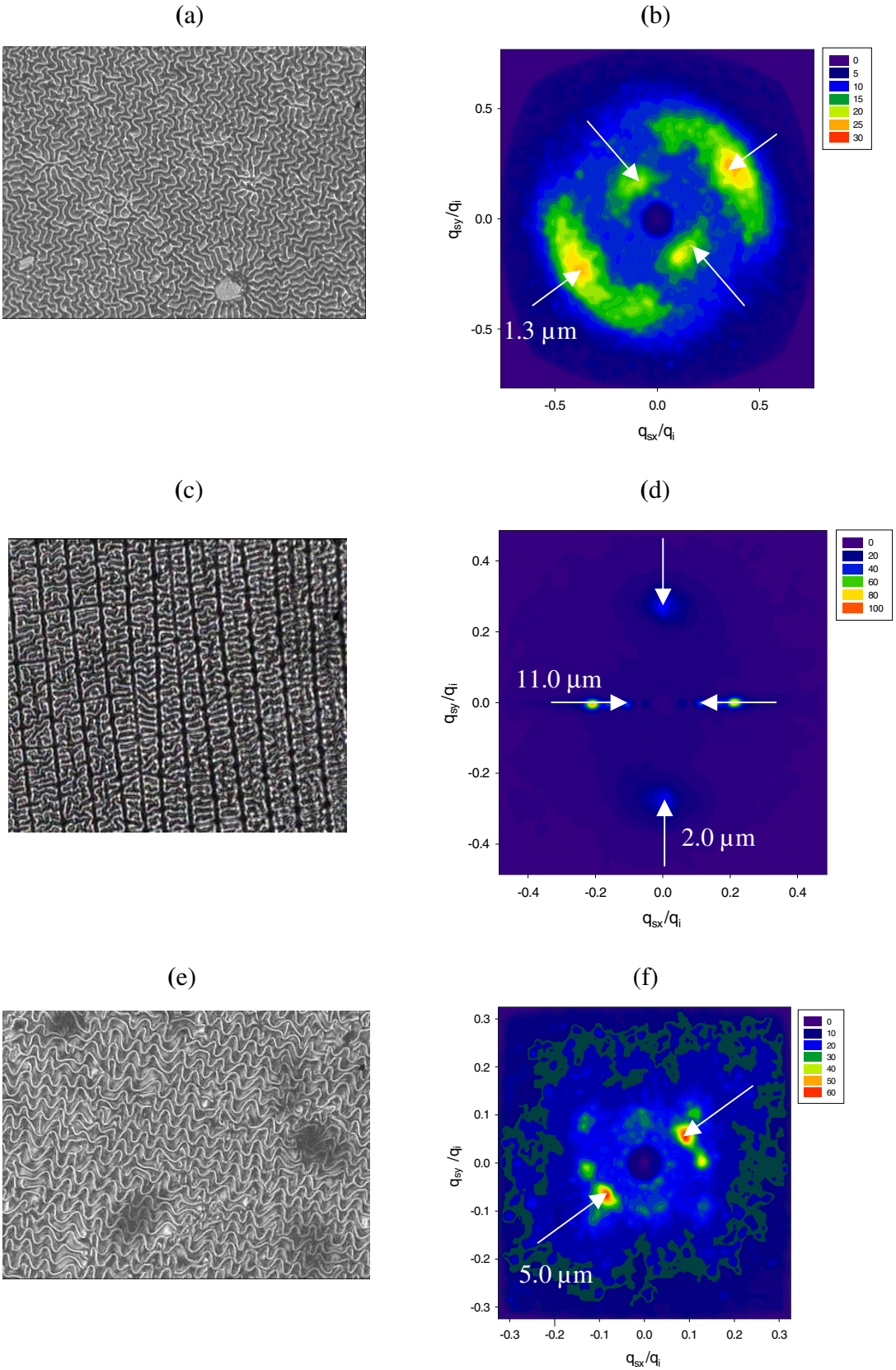

Fig. 4. POM images ((a), (c) and (e)) and SALS patterns ((b), (d) and (f)). (a) and (b): *sample III-20* (originating from *sample II0* after extraction with toluene and drying). (c) and (d): *sample III-2A* (originating from *sample IIA*, followed by extraction with toluene). (e) and (f): *sample III-2B* (originating from *sample IIB* followed by extraction with toluene and drying).

Films of any type can then be in one of three different states:

- *State 0*: the film has not been subjected to any mechanical stress or deformation.
- *State A*: the film was subjected to a plane uniaxial stress along $\mathbf{d}_1$, this was removed, then a plane uniaxial stress was applied along $\mathbf{d}_2$, finally this was also removed.
- *State B*: the film in state A was subjected to a plane uniaxial stress along $\mathbf{d}_1$, which was subsequently removed.

By combining the above, we are henceforth able to reference our films in a particularly compact and convenient manner: thus *sample I0* means a type-I film in state 0, *sample-IIA* is a type-II film in state A, *sample III-2B* is a type-III-2 film in state B, etc.

3 Results and discussion

We started by looking at the effect of UV irradiation on film properties.

The shear-induced anisotropy of the as-cast film (*sample I0*) is reflected in the values of its Young's modulus measured in the direction of casting shear (*i.e.*, along $\mathbf{d}_1$), $E_{\mathrm{I0}}(\mathbf{d}_1) = 4.22\,\mathrm{MPa}$, and perpendicular to the direction of casting shear (*i.e.*, along $\mathbf{d}_2$), $E_{\mathrm{I0}}(\mathbf{d}_2) = 2.84\,\mathrm{MPa}$ (see Table 1). UV irradiation of this sample yields *sample II0*: the resulting higher cross-linking density leads to the moduli being larger than for (unirradiated) sample I0: $E_{\mathrm{II0}}(\mathbf{d}_1) = 4.39\,\mathrm{MPa}$ and $E_{\mathrm{II0}}(\mathbf{d}_2) = 3.29\,\mathrm{MPa}$. It was recently pointed out [25] that UV exposure, by reinforcing the links between the hard and soft parts of the segregated copolymer for these kinds of elastomer, gives rise to a different molecular organisation that is reflected in their mechanical properties.

The free surface of the films was observed before (*sample I0*) and after (*sample II0*) UV irradiation, in the absence of applied stresses; Figure 3 shows the 3D topography image ($50 \times 50\,\mu\mathrm{m}^2$ scan) of the nanometrically flat surface of sample II0. This is characterised by the roughness parameters listed in Table 2. A similarly flat topography was obtained for elastomer films removed from the substrate and subjected to plane uniaxial stresses, but not exposed to UV radiation (*samples IA* or *IB*).

We next investigated how textures can be produced and controlled by solvent and/or mechanical treatments.

The irradiated film (*sample II0*) was extracted in toluene for 36 hours, yielding *sample III-20*. This sample was observed under parallel polars (see Fig. 4a) and the POM image, obtained with the microscope focused near the surface, reveals a texture of long corrugated, randomly distributed line-like textures. The spacing between these structures shows periodicity (about $2.7\,\mu\mathrm{m}$). The rich pattern revealed by SALS (see Fig. 4b) exhibits two well-defined periodicities, one corresponding to that observed by POM and another (about $1.3\,\mu\mathrm{m}$) that might be attributed to ordering of the material in the bulk, also induced by the strain generated during swelling. It is not detected by AFM, which probes the surface only, but exclusively by SALS, which examines the whole thickness of the film. SALS measurements performed on different regions of the sample show that while the characteristic periodicity length scales remain in the same range, the preferential orientation changes from region to region. This behaviour suggests that although orientational order exists over one typical diameter of the SALS laser spot (around 1.5 mm), orientational correlations do not extend across the whole sample. The orientational order suggested by SALS at sub-mm scale is visible in the POM image.

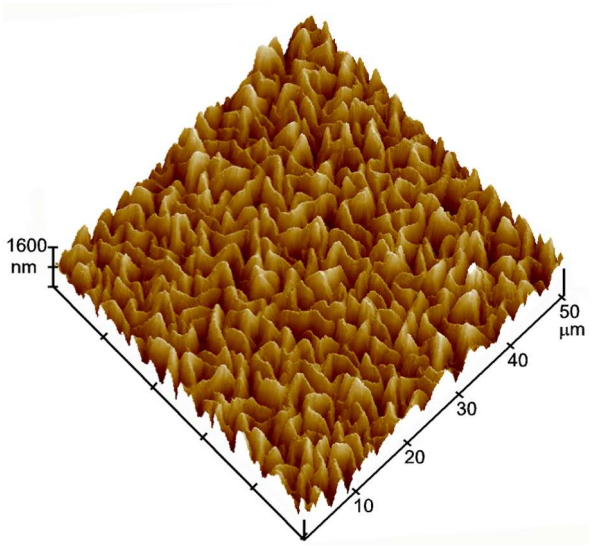

Fig. 5. 3D topography image ($50 \times 50\,\mu\mathrm{m}^2$ scan) of the free surface of *sample III-20*, which was obtained from *sample II0* after extraction with toluene. The sample surface is corrugated, with μm-sized features along all axes, resulting in a dramatic increase in all roughness parameters, see Table 2.

To single out the effect of UV irradiation, the film with no UV exposure (*sample I0*) was also extracted in toluene, giving a different *sample III-10*, with a flat surface. We are thus led to the conclusion that UV irradiation changes the properties of a thin layer on the upper surface of the elastomer film that is responsible for the periodic modulations described above (recall that the film thickness is much greater than the typical amplitude of the modulations: there is no question of the whole film wrinkling, just a thin surface layer). The bottom surface of the film, which was not exposed to UV radiation, is indeed flat. Figure 5 shows the irradiated corrugated surface of *sample III-20*, with μm-sized features along all axes, resulting in a dramatic increase in all roughness parameters, see Table 2. The spacing between surface features found by AFM, about $2.7\,\mu\mathrm{m}$, is in agreement with the POM results.

Sample III-20, with a surface topography characterised by randomly distributed patterns, is much less elastically anisotropic than *samples I0* or *II0*, as can be seen from Table 1: $E_{\text{III-20}}(\mathbf{d}_1) = 3.73\,\mathrm{MPa}$ and $E_{\text{III-20}}(\mathbf{d}_2) = 3.76\,\mathrm{MPa}$.

In order to investigate the effect of mechanical fields upon the surface topography of the irradiated samples, *sample II0* was subjected to a (elastic) uniaxial

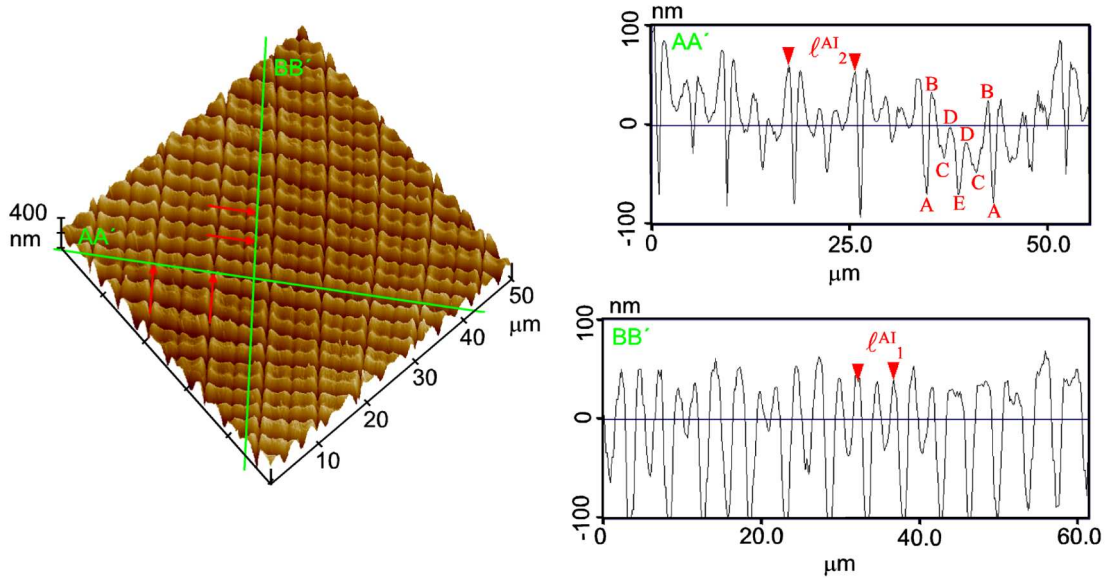

Fig. 6. 3D topography image ($50 \times 50\,\mu m^2$ scan) of the free surface of *sample IIA*, which was obtained by subjecting *sample II0* to uniaxial plane stresses along $\mathbf{d}_1$ and $\mathbf{d}_2$ consecutively. The AA′ and BB′ cross-sections were taken along the lines marked on the 3D image. AA′ was taken along $\mathbf{d}_2$ and BB′ along $\mathbf{d}_1$. See the text for details.

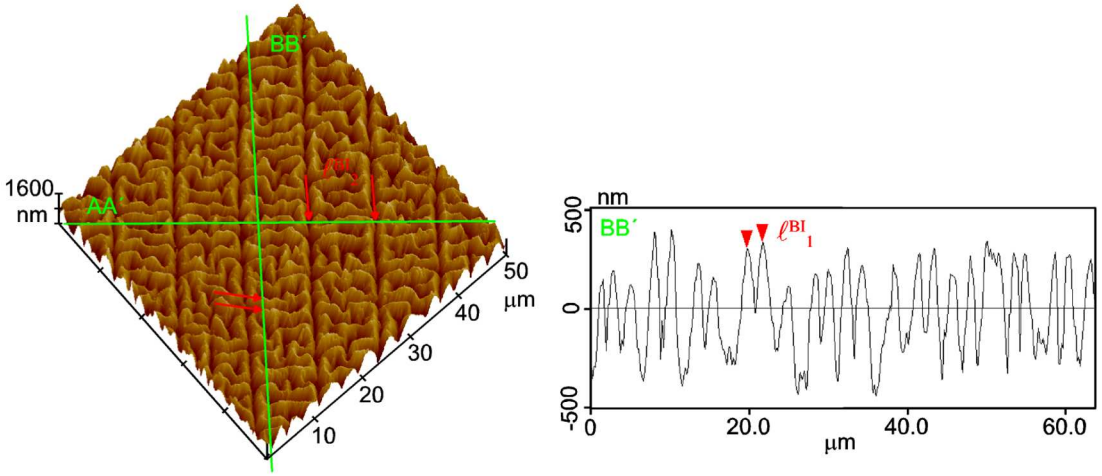

Fig. 7. 3D topography image ($50 \times 50\,\mu m^2$ scan) of the free surface of *sample III-2A*, which was obtained by extracting *sample IIA* in toluene. The BB′ cross-section was taken along the lines marked on the 3D image; it is along $\mathbf{d}_1$. See the text and Table 2 for details.

deformation $\varepsilon_1 = 0.2$ along $\mathbf{d}_1$ by applying stress $\sigma_1 = 0.88\,MPa$ (see [31] for typical stress-strain curves). After removal of this stress a periodic pattern ("bands") developed on the elastomer film surface with wave vector parallel to $\mathbf{d}_1$. Then an (elastic) extensional deformation $\varepsilon_2 = 0.2$ was imposed along $\mathbf{d}_2$ by means of stress $\sigma_2 = 0.66\,MPa$, which was subsequently removed, yielding *sample IIA*. The surface topography of *sample IIA* is shown in Figure 6. It is characterised by two periodic modulations with wave vectors parallel to $\mathbf{d}_1$ and $\mathbf{d}_2$. The AFM height profile along $\mathbf{d}_1$ (Fig. 6, cross-section BB′) has spatial periodicities ℓ_1 ranging from 4 to 5 μm; the peak-to-valley heights are alternately $h_{11} = 65 \pm 16\,nm$ and $h_{12} = 160 \pm 30\,nm$. In contrast, the AFM height profile along $\mathbf{d}_2$ (Fig. 6, cross-section AA′) reveals a complex periodic structure that repeats with a spatial periodicity ℓ_2 in the range from 7.9 to 8.6 μm. Within this period a symmetric sequence of nine peaks is always observed with the order ABCDEDCBA (shown in the AA′ cross-section), where the peak-to-valley height varies between 30 and 60 nm.

Next we looked at how extraction in toluene changes the topography of a film that was previously deformed. *Sample IIA* was extracted in toluene yielding *sample III-2A*. This was observed under parallel polars (Fig. 4c) and its POM image reveals a randomly distributed line-like corrugated texture with a similar periodicity (2 μm) as found in *sample III-20*. Besides this, another periodicity is present (11 μm) with wave vector along $\mathbf{d}_1$. In the SALS pattern (Fig. 4d) the arrows indicate the position of the first-order scattering peaks corresponding to the two main

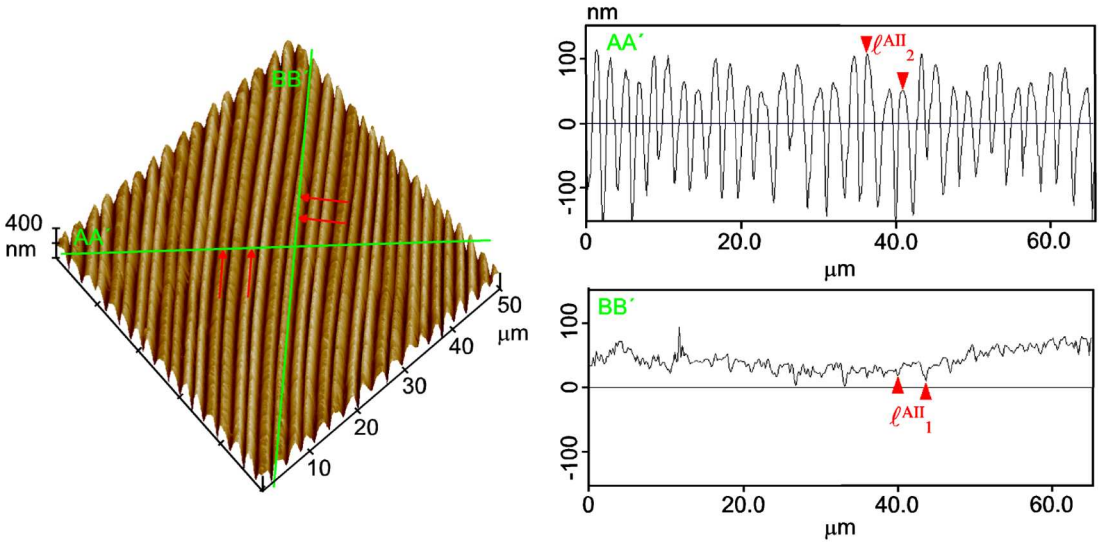

Fig. 8. 3D topography image ($50 \times 50\,\mu m^2$ scan) of the free surface of *sample IIB*, obtained by subjecting *sample IIA* to stress along $\mathbf{d}_1$. The roughness parameters are listed in Table 2. Spatial periodicities can be observed along $\mathbf{d}_1$ (cross-section AA′) and along $\mathbf{d}_2$ (cross-section BB′); the latter reveals the imprint of state A. See the text for details.

periodicities previously observed by POM. The second periodicity (11 μm) may be attributed to the mechanical treatment the sample was subjected to before extraction in toluene: it is not present in the unstrained samples, and is detected by both POM and SALS. The 3D topography image of *sample III-2A* is shown in Figure 7. The corresponding roughness parameters are also collected in Table 2. The two main periodicities found by POM and SALS can also be found by AFM, $\ell_1 = 2 \pm 1.5\,\mu$m and $\ell_2 = 10 \pm 0.5\,\mu$m (Fig. 7, cross-sections BB′ and AA′, respectively).

As can be seen from Table 1, *sample III-2A* is also elastically less anisotropic, $E_{\text{III-2A}}(\mathbf{d}_1) = 3.93$ MPa and $E_{\text{III-2A}}(\mathbf{d}_2) = 3.70$ MPa, than *sample II0*, but more so than *sample III-20*. This is compatible with the fact that the precursor of *sample III-2A*, *sample IIA*, has residual order induced by the mechanical fields, whereas the precursor of *sample III-20*, *sample II0*, has not.

It is also interesting to research whether such mechanically imprinted textures are permanent, or can be further modified. To this end we obtained *samples in state B* by applying an extension along $\mathbf{d}_1$ to *samples in state A*. Figure 8 shows the 3D topography image of the free surface of *sample IIB*, which is characterised by an increase in the roughness parameters relative to *sample II0*, see Table 2. A spatial modulation can be observed along $\mathbf{d}_1$ (cross-section AA′). Within this modulation the peaks are grouped in pairs: each pair repeats with period $\ell_1 = 4.5 \pm 0.2\,\mu$m. The peak-to-valley height in the gap between peaks of different heights is $h_{11} = 220 \pm 70$ nm and the peak-to-valley heights in the gap between peaks of similar heights are $h_{12} = 120 \pm 30$ nm and $h_{13} = 200 \pm 50$ nm for the lower (darker) and higher (brighter) peaks, respectively. The peak-to-peak height difference between consecutive peaks of different heights is constant and equal to $h_{14} = 40 \pm 20$ nm. The profile along $\mathbf{d}_2$ (cross-section BB′) reveals the imprint of the precursor of *sample IIB*, *sample IIA*, with characteristic period $\ell_2 = 2.4 \pm 0.3\,\mu$m and peak-to-valley height $h_2 = 15 \pm 5$ nm.

Sample III-2B was obtained by extracting *sample IIB* in toluene. *Sample III-2B* was observed under parallel polars (Fig. 4e) and the POM image reveals corrugated patterns that tend to pack in a sinusoidal manner with wave vector along $\mathbf{d}_2$. The peak-to-peak distance of the sinusoid-like corrugations is around 5 μm as found from the SALS pattern and marked by the arrows in Figure 4f. *Sample III-2B* has more anisotropic tensile properties than *samples III-20* or *III-2A*, see Table 1: $E_{\text{III-2B}}(\mathbf{d}_1) = 3.57$ MPa and $E_{\text{III-2B}}(\mathbf{d}_2) = 2.47$ MPa, which may be a consequence of the fact that its precursor, *sample IIB*, has a high degree of order induced by the mechanical field. However, these are the lowest moduli of all the samples we prepared.

Figure 9 shows the 3D topography image of the free surface of *sample III-2B*, which is characterised by an increase in the roughness parameters relative to *samples IIB* (its precursor), *III-20* and *III-2A*, see Table 2. The wave vector of the corrugation varies along the AFM height profile along $\mathbf{d}_1$ (Fig. 9, cross-section AA′). The peak-to-peak periodicity $\ell_1 = 2.0 \pm 0.5\,\mu$m is indicated on cross-section AA′, it is of the same order of magnitude as the period imprinted on the sample after UV irradiation (*i.e.*, on *sample II0*). The solid wavy line in the 3D topography image is a sinusoid-like corrugation imprinted on the surface, also observed by POM.

Finally, Figure 10 summarises our experimental procedures and findings, as well as the notation for naming samples. The very important fact should be highlighted that a sample of *type II* (*i.e.*, UV-irradiated) can be reversibly switched between states A and B by the application of a stress σ_1 along $\mathbf{d}_1$ (A to B) or σ_2 along $\mathbf{d}_2$ (B to A). Alternatively, states *IIA* or *IIB* can be erased, giving state *II0*, by raising the sample temperature above 65 °C. At room

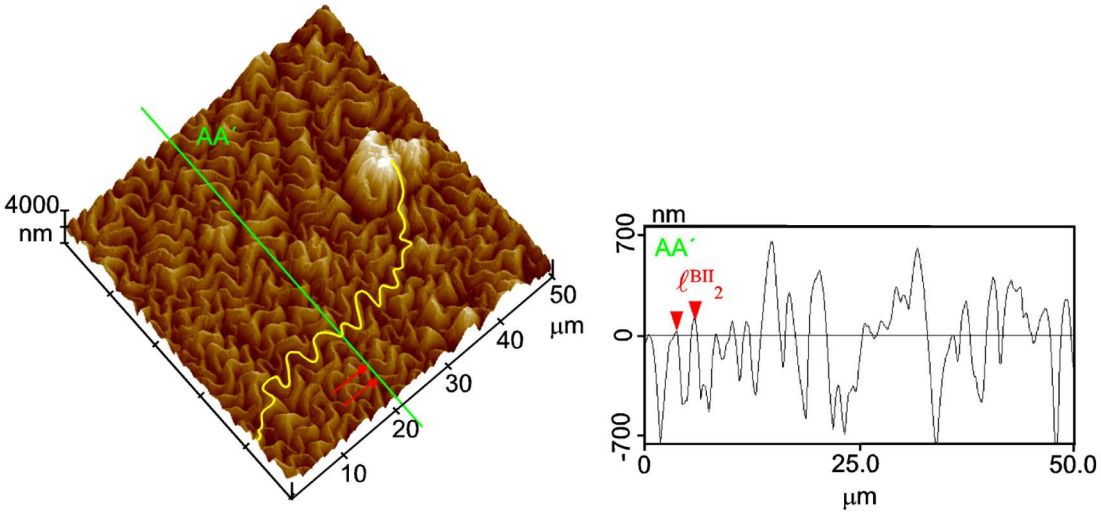

Fig. 9. 3D topography image ($50 \times 50\,\mu m^2$ scan) of the free surface of *sample III-2B*, which was obtained by extracting *sample IIB* in toluene. The roughness parameters are listed in Table 2. The AFM height profile along $\mathbf{d}_1$, represented in cross-section AA′, displays a periodicity. A sinusoid-like corrugation is shown as a solid wavy line in the 3D topography image. See the text for details.

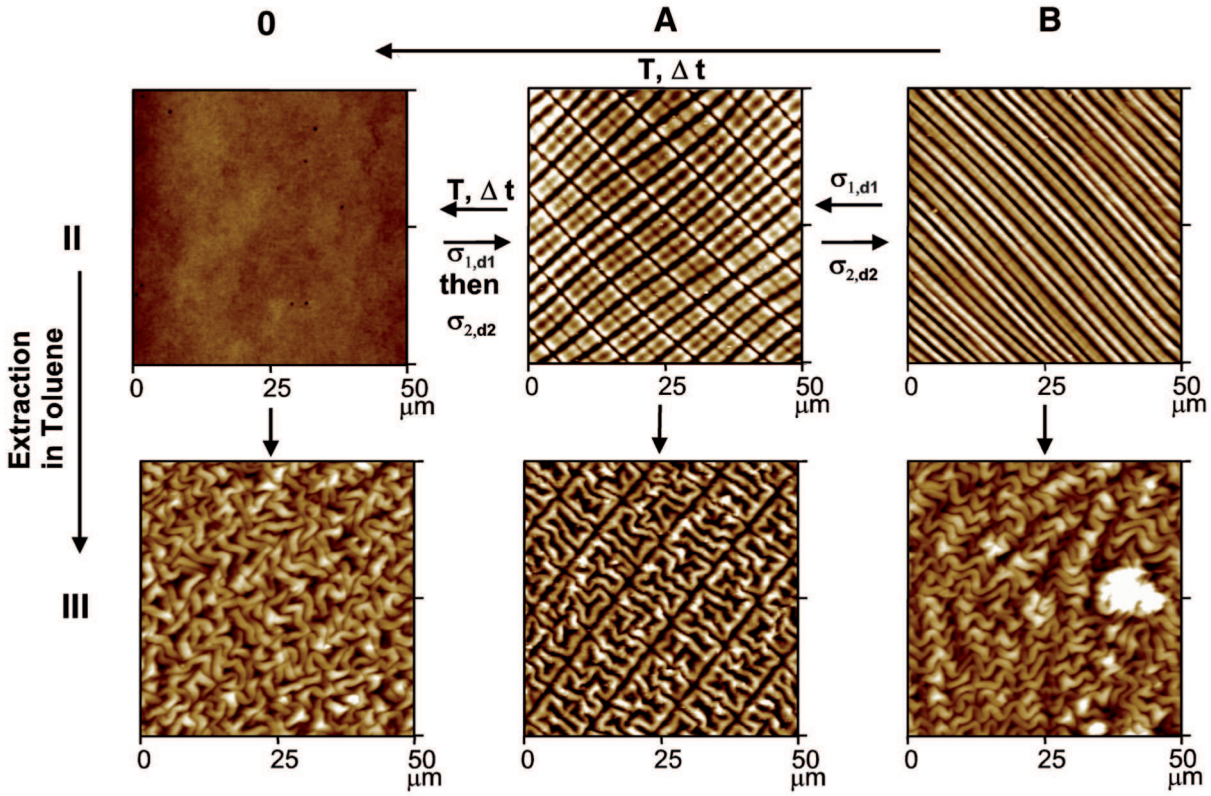

Fig. 10. Schematic diagram of the topography images of the free surface of the 60% PU/40% PBDO elastomer film. *Type-II samples* are samples that have been exposed to UV radiation ($\lambda = 254\,nm$) for two days. *Type-III-2 samples* originate from type-II samples after extraction in toluene. A sample is said to be in *state 0* if it has not been subjected to mechanical treatment. *Sample IIA* (a type-II sample in state A) is obtained by subjecting *sample II0* (a type-II sample in state 0) to sequential extensions along $\mathbf{d}_1$, upon applying the stress $\sigma_1 = 0.22\,MPa$, and along $\mathbf{d}_2$, upon applying the stress $\sigma_2 = 0.19\,MPa$. *Sample IIB* (a type-II sample in state B) is obtained from *sample IIA* (a type-II sample in state A) after an extension along $\mathbf{d}_2$ upon applying the stress σ_2. Samples of type II can be switched between states A and B by applying/removing σ_1 along $\mathbf{d}_1$ (A $\rightarrow$ B) and σ_2 along $\mathbf{d}_2$ (B $\rightarrow$ A), respectively. States A and B can be erased, giving state 0, by raising the temperature above 65 °C, or by waiting at room temperature for a time that depends on the rate of extension.

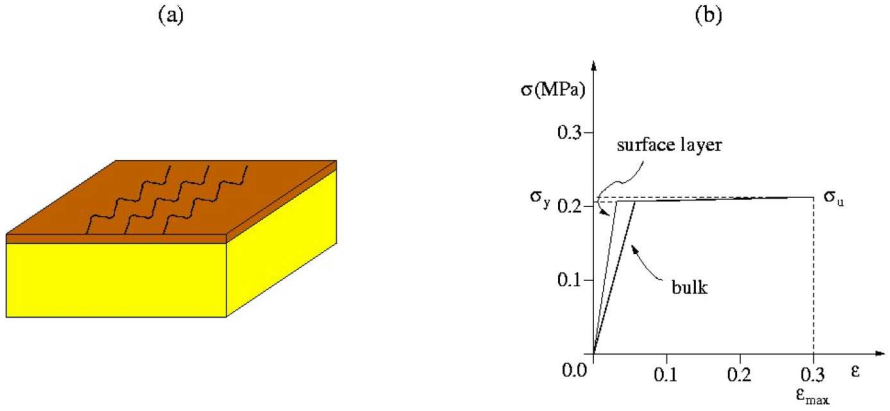

Fig. 11. (a) Schematic representation of the "upper crust" model: a thin, stiff layer atop a thick, softer substrate. (b) Stress-strain curves for the thin layer and for the substrate (bulk). Technical reasons require that the plastic region of the curves should have a small, finite slope; this is shown exaggerated for clarity.

temperature, these states decay with a time constant that is a function of the rate of extension which was used to produce them; in all cases state *II0* is recovered after at most a few months.

However, no such reversible switching is possible between states *III-2A* and *III-2B*: swelling in toluene freezes the imprinted patterns permanently on the film surfaces.

Currently we are not able to explain the 1.3 μm and 11 μm periodicities found in samples *III-20* and *III-2A*, respectively, as the experimental techniques that we have used so far do not yield enough information on them. We are looking into the possibility of elucidating their nature by means of transmission electron microscopy (TEM), as done in, *e.g.*, [37].

All the results reported in this section were found to be highly reproducible for the same sample preparation conditions and subsequent treatments.

4 Modelling

We start by noting that the corrugations that we have observed have amplitudes (of the order of tens or hundreds of nm) much smaller than the film thickness ($\sim 100\,\mu$m). Furthermore, the film surface not exposed to UV did not exhibit any features. This suggests that the effect of UV irradiation is to modify the properties of a relatively thin layer on the film surface. This layer will likely have a higher density of cross-links and therefore it will be stiffer, which is consistent with the data in Table 1: UV-irradiated *sample II0* indeed has higher elastic moduli than unirradiated *sample I0*. The change is, however, not large, 4–16% depending on direction, which hints at a surface layer thickness (provided the same can be defined unambiguously) of a few percent of the total film thickness.

In a recent paper, Cerda and Mahadevan [38] addressed the wrinkling of a thin, stiff elastic layer sitting atop a thicker, softer substrate. They found that two different types of wrinkling can occur. First, when the system is stretched by clamping its boundaries, it is not able to contract laterally close to the clamps, as is required to do to conserve volume. This sets up a biaxial state of stress that is compressive away from the clamped boundaries, which leads to buckling with wave vector perpendicular to the direction of stretching. Second, when the natural dimensions of the thin surface layer are greater than those of the underlying substrate, then the thin surface layer will buckle. In both cases buckling prevails because a thin elastic plate finds it cheaper to bend rather than compress [39]. The wavelength of the resulting corrugation is determined by the competition between the bending stiffness of the thin film on top (which penalises short wavelengths) and the energy of stretching the substrate below (which penalises long wavelengths); from [40], $\lambda \propto t(E_l/E_b)^{1/3}$, where E_l is Young's modulus of the surface layer of thickness t, and E_b that of the substrate (bulk).

On the basis of the above we propose the following model for explaining our results:

1. The stripes reported in earlier papers [31,32,34,35] are just Cerda and Mahadevan's "wrinkles in a plastic sheet": they are parallel to the direction of applied stress and have small amplitude.
2. On stretching the elastomer, the surface layer, being stiffer, deforms plastically by more than the substrate. So, on removing the stress, the natural dimensions of the surface layer and of the substrate are now mismatched, hence the bands. A similar effect was recently reported by Efimenko *et al.* for a PDMS film [40]. This is also consistent with the fact that one can switch reversibly between *samples IIA* and *IIB*, and that the surface textures of these samples can be erased by either heating them to 65 °C, or waiting for long enough at room temperature, which is suggestive of recovery due to viscoelastic flow of a plastically deformed state. One further supporting argument is the fact that many of the periodic surface patterns (*e.g.*, that of *sample IIB*) are characterised by more than one wavelength: indeed such a buckling "cascade" has been reported by other authors [40,41] in cases where a plastically deformed thin sheet has to relieve a compressive stress. As the sheet buckles its effective thickness changes, so a new wavelength of instability is selected.

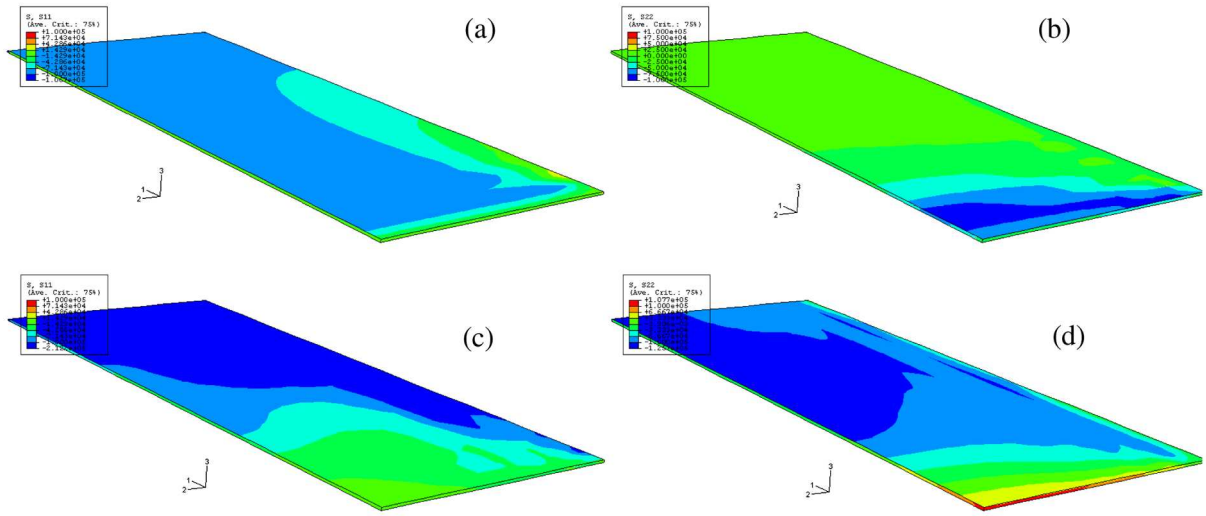

Fig. 12. Distribution of residual stresses σ_1 ((a), (c)) and σ_2 ((b), (d)) in our model elastomer film. (a) and (b): after application and release of stress $\sigma_1 = 0.88\,\mathrm{MPa}$ along $\mathbf{d}_1$ (parallel to the long edge of the samples) to the undeformed elastomer; (c) and (d): after application and release of stress $\sigma_2 = 0.19\,\mathrm{MPa}$ along $\mathbf{d}_2$ (parallel to the short edge of the samples) to the elastomer previously stressed along $\mathbf{d}_1$. Only one quarter of the film is shown: the top edge and the near edge are in the planes of symmetry, see the text for details.

Table 3. Parameters used in the Finite Elements simulation. Bulk Young's modulus from *sample I0*, see Table 1. We neglected the elastic anisotropy at this stage.

	Surface layer	Bulk
Young's modulus (MPa)	5.92	4.22
Poisson's ratio	0.49	0.49
Yield stress (MPa)	0.220	0.220
Ultimate stress (MPa)	0.221	0.221
Maximum total strain	0.30	0.30

We carried out simulations of this model using the Finite Element package ABAQUS [42]. We assumed the surface layer to comprise about 10% of the film thickness and estimated its elastic modulus from the data of Table 1 for *samples I0* and *II0*, approximating our system as a composite of layer + substrate under same-strain conditions (see Fig. 11a). The simplest plastic behaviour was assumed: a nearly flat stress-strain curve past the yield stress, which was taken to be the same for both surface and bulk material (see Fig. 11b and Tab. 3 for the parameters used in the simulations). The films have two planes of mirror symmetry, along and perpendicular to the direction of stretching, hence only one quarter of the domain was modelled. Appropriate boundary conditions were applied in the two symmetry planes and rigid-body motion was prevented by additionally fully constraining the lower node common to these planes. In addition, nodes pertaining to a surface where stress is applied are constrained, during application of stress, so as not to allow translation in the respective plane. This mimics the fact that a film is stretched by clamping two of its edges, which therefore are not free to deform, leading to non-uniform strains/stresses. Because the surface material is stiffer than the bulk, it will enter the plastic regime earlier and upon unloading (for the same final elongation, see Fig. 11b) will retain a larger plastic strain. Figure 12 shows the distribution of stresses σ_1 and σ_2 in the elastomer film after stress was applied sequentially along $\mathbf{d}_1$ (Figs. 12a, b) and $\mathbf{d}_2$ (Figs. 12c, d). There is a clear differential response along the layer thickness: upon release of the applied stress, the surface layer is in compression, whereas the bulk is mostly under traction. Compression of the surface layer is conducive to the occurrence of undulations associated with elastic instabilities. There remains to extract the wavelengths of these surface undulations. This work is in progress and will be reported elsewhere.

Our modelling is, of course, at a very preliminary stage. Indeed, we do not know at present whether there is a sharp transition between the surface layer and the substrate and, if so, what is the thickness of the former, which we have treated as a free parameter. We have only proposed a simple mechanism whereby bands *may* form, and shown that it is plausible —we have not determined their equilibrium amplitude(s) or wavelength(s). Nor have we explained why the bands disappear after a few months; this, as well as the kinetics of their formation, will very likely require a model for an elastic film on a viscoelastic substrate, such as that recently proposed by Huang and Suo [43,44]. At the moment, we do not have enough data to allow a detailed comparison with this theory, which would require knowledge of i) the band wavelengths and amplitudes as a function of the applied strains, for which we have only a few data points, ii) the thickness of the surface layer and iii) the time evolution of the band wavelengths and amplitudes over the very short interval (less than 1 second) in which they form, as well as over the very long interval (several months) in which they disappear. We have also

completely neglected the elastic anisotropy of the samples, which might explain, on the basis of the simple theory of [40], why the bands have different wavelengths along $\mathbf{d}_1$ and $\mathbf{d}_2$. Finally, the role of swelling in freezing/erasing surface textures remains poorly understood.

5 Conclusions

In this work we describe for the first time an elastomeric material with different functionalities resulting from the textures generated by UV irradiation of one of its surfaces. The synthesis is straightforward and uses current chemicals and methods; no sophisticated deposition or emulsification steps are necessary. A tuneable topographic system can be obtained from a single formulation of a urethane/urea elastomer upon the application of a mechanical field and/or solvent extraction. The topographies, with amplitudes in the tens of nm range and periods of a few μm, are remarkably defect-free over distances of the order of a few mm, and can be switched between themselves reversibly, without any cracks appearing. If left unstressed, an imprinted pattern has a lifetime of a few months.

The as-cast sheared elastomer exhibits the most anisotropic tensile properties, while the toluene-extracted irradiated elastomer exhibits the least anisotropic mechanical properties. In general the process of extraction in toluene decreases the tensile anisotropy, but this decrease can be hampered by the presence of a periodicity in the precursor film. A full understanding of this mechanism, as well as of the different periodicities present, requires further work, possibly using TEM.

The observed behaviour seems to have its origin in the shear-casting film preparation conditions combined with the UV-induced changes at the molecular level in the top film layer directly exposed, as in other systems discussed in the literature [10,38].

This work was supported by Projects POCI/CTM/56382/2004-FEDER and POCTI/CTM/42456/2001-FEDER, and by *Portuguese Science Foundation* (FCT) through Pluriannual Contracts with CENIMAT and ICEMS. We thank M. Warner for hospitality and many insightful discussions.

References

1. C. Koulic, R. Jérôme, Macromolecules **37**, 888 (2004).
2. T.L. Morkved, M. Lu, A.M. Urbas, E.E. Ehrichs, H.M. Jaeger, P. Mansky, T.P. Russel, Science **931**, 273 (1996).
3. M. Camacho-Lopez, H. Finkelmann, P. Palffy-Muhoray, M. Shelley, Nat. Mater. **3**, 307 (2004).
4. G. Evmenenko, C.J. Yu, S. Kewalramani, P. Dutta, Langmuir **20**, 1698 (2004).
5. N. Bowden, S. Brittain, A.G. Evans, J.W. Hutchinson, G.M. Whitesides, Nature **393**, 146 (1998).
6. N. Stutzmann, T.A. Tervoort, K. Bastiaansen, P. Smith, Nature **407**, 613 (2000).
7. M. Watanabe, H. Shirai, T. Hirai, J. Appl. Phys. **92**, 4631 (2002).
8. S.R. Quake, A. Scherer, Science **290**, 1536 (2000).
9. N.A. Peppas, R. Langer, Science **263**, 1715 (1994).
10. W.T.S. Huck, N. Bowden, P. Onck, T. Pardoen, J.W. Hutchinson, G.M. Whitesides, Langmuir **16**, 3497 (2000).
11. S.P. Lacour, S. Wagner, Z. Huang, Z. Suo, Appl. Phys. Lett. **82**, 2404 (2003).
12. P.J. Yoo, H.H. Lee, Phys. Rev. Lett. **91**, 154502 (2003).
13. P.J. Yoo, K.Y. Suh, H. Kang, H.H. Lee, Phys. Rev. Lett. **93**, 034301 (2004).
14. J.S. Sharp, R.A.L. Jones, Phys. Rev. E **66**, 011801 (2002).
15. J.S. Sharp, D. Vader, J.A. Forrest, M.I. Smith, M. Khomenko, K. Dalnoki-Veress, Eur. Phys. J. E **19**, 423 (2006).
16. C. Jiang, S. Markutsya, V.V. Tsukruk, Adv. Mater. **16**, 157 (2004).
17. C. Jiang, S. Markutsya, Y. Pikus, V.V. Tsukruk, Nat. Mater. **3**, 721 (2004).
18. S.L. Cooper, A.V. Tobolsky, J. Appl. Polym. Sci. **10**, 1837 (1966).
19. I.D. Fridman, E.L. Thomas, Polymer **21**, 388 (1980).
20. F. Yeh, B.S. Hsiao, B.B. Sauer, S. Michel, H.W. Siesler, Macromolecules **36**, 1940 (2003).
21. M.J. O'Sickel, B.D. Lawrey, G.L. Wilkes, J. Appl. Polym. Sci. **84**, 229 (2002).
22. M. Hasegawa, T. Ikawa, M. Tsuchimori, O. Watanabe, Y. Kawata, Macromolecules **34**, 7471 (2001).
23. C. Park, J. Yoon, E.L. Thomas, Polymer **44**, 6725 (2003).
24. E.A. Moschou, S.F. Peteu, L.G. Bachas, M.J. Madou, S. Daunert, Chem. Mater. **16**, 2499 (2004).
25. M. Park, C. Harrison, P.M. Chaikin, R.A. Register, D.H. Adamson, Science **276**, 1401 (1997).
26. L. Leibler, Macromolecules **13**, 1602 (1980).
27. A.L. Gamboa, E.J.M. Filipe, P. Brogueira, Nano Lett. **2**, 1083 (2002).
28. T. Kaneko, K. Yamaoka, Y. Osada, J.P. Gong, Macromolecules **37**, 5385 (2004).
29. J. Fu, B. Luan, X. Yu, Y. Cong, J. Li, C. Pan, Y. Han, Y. Yang, B. Li, Macromolecules **37**, 976 (2004).
30. D.P. Queiroz, M.N. de Pinho, C. Dias, Macromolecules **36**, 4195 (2003).
31. A.C. Trindade, M.H. Godinho, J.L. Figueirinhas, Polymer **45**, 5551 (2004).
32. M.H. Godinho, J.L. Figueirinhas, C.-T. Zhao, M.N. de Pinho, Macromolecules **33**, 7675 (2000).
33. M. Warner, E.M. Terentjev, *Liquid Crystal Elastomers* (Clarendon Press, Oxford, 2003).
34. M.H. Godinho, L.V. Melo, P. Brogueira, Mater. Sci. Eng. C **23**, 919 (2003).
35. M.H. Godinho, A.C. Trindade, J.L. Figueirinhas, D. Vidal, L.V. Melo, P. Brogueira, Synth. Met. **147**, 209 (2004).
36. C.T. Zhao, M.N. de Pinho, Polymer **40**, 6089 (1999).
37. D.P. Queiroz, M.C. Gonçalves, M.N. Pinho, J. Appl. Polym. Sci. **103**, 315 (2007).
38. E. Cerda, L. Mahadevan, Phys. Rev. Lett. **90**, 074302 (2003).
39. L.D. Landau, L.M. Lifshitz, *Theory of Elasticity*, 3rd ed. (Pergamon Press, New York, 1986).
40. K. Efimenko, M. Rackaitis, E. Manias, A. Vaziri, L. Mahadevan, J. Genzer, Nat. Mater. **4**, 293 (2005).
41. E. Sharon, B. Roman, M. Marder, G.-S. Shin, H.L. Swinney, Nature **419**, 579 (2002).
42. `http://www.abaqus.com` or `http://www.hks.com`.
43. R. Huang, Z. Suo, Int. J. Solids Struct. **39**, 1791 (2002).
44. R. Huang, J. Mech. Phys. Solids **53**, 63 (2005).